

# Role of multi-electron effects in the asymmetry of strong-field ionization and fragmentation of polar molecules: The methyl halide series

## Journal Article

### Author(s):

Walt, Samuel G.; Ram, N. Bhargava; von Conta, Aaron; Tolstikhin, Oleg I.; Madsen, Lars Bojer; Jensen, Frank; Wörner, Hans Jakob

### Publication date:

2015-12-10

### Permanent link:

<https://doi.org/10.3929/ethz-a-010779427>

### Rights / license:

[In Copyright - Non-Commercial Use Permitted](#)

### Originally published in:

The Journal of Physical Chemistry A 119(49), <https://doi.org/10.1021/acs.jpca.5b07331>

# Role of Multi-Electron Effects in the Asymmetry of Strong-Field Ionization and Fragmentation of Polar Molecules: The Methyl Halide Series

Samuel G. Walt,<sup>†</sup> N. Bhargava Ram,<sup>†</sup> Aaron von Conta,<sup>†</sup> Oleg I. Tolstikhin,<sup>‡</sup>  
Lars Bojer Madsen,<sup>¶</sup> Frank Jensen,<sup>§</sup> and Hans Jakob Wörner<sup>\*,†</sup>

<sup>†</sup>*Laboratorium für Physikalische Chemie, ETH Zürich, 8093 Zürich, Switzerland*

<sup>‡</sup>*Moscow Institute of Physics and Technology, Dolgoprudny 141700, Russia*

<sup>¶</sup>*Department of Physics and Astronomy, Aarhus University, DK-8000 Aarhus C, Denmark*

<sup>§</sup>*Department of Chemistry, Aarhus University, DK-8000 Aarhus C, Denmark*

E-mail: hwoerner@ethz.ch

## Abstract

We report angle- and momentum-resolved measurements of the dissociative ionization and Coulomb explosion of methyl halides ( $\text{CH}_3\text{F}$ ,  $\text{CH}_3\text{Cl}$ ,  $\text{CH}_3\text{Br}$ ,  $\text{CH}_3\text{I}$ ) in intense phase-controlled two-color laser fields. At moderate laser intensities we find that the emission asymmetry of low-energy  $\text{CH}_3^+$  fragments from the  $\text{CH}_3^+ + \text{X}^+$  ( $\text{X} = \text{F}, \text{Cl}, \text{Br}, \text{I}$ ) channel reflects the asymmetry of the highest occupied molecular orbital of the neutral molecule with important contributions from the Stark effect. This asymmetry is correctly predicted by the weak-field asymptotic theory, provided that the Stark effect on the ionization potentials is calculated using a non-perturbative multi-electron approach. In the case of high laser intensities we observe a reversal of the emission asymmetries for high-energy  $\text{CH}_3^+$  fragments, originating from the dissociation of  $\text{CH}_3\text{X}^{q+}$  with  $q \geq 2$ . We propose ionization to electronically-excited states to be at the origin of the reversed asymmetries. We also report the measurements of the emission asymmetry of  $\text{H}_3^+$  which is found to be identical to that of the low-energy  $\text{CH}_3^+$  fragments measured at moderate laser intensities. All observed fragmentation channels are assigned with the help of CCSD(T) calculations. Our results provide a benchmark for theories of strong-field processes and demonstrate the importance of multi-electron effects in new aspects of the molecular response to intense laser fields.

## Introduction

The ionization of molecules in strong laser fields is the common first step of several new techniques for probing the dynamics of molecules. Understanding the ionization process is therefore essential for the further development of high-harmonic spectroscopy,<sup>1-6</sup> laser-induced electron diffraction<sup>7-10</sup> and strong-field photoelectron holography.<sup>11-13</sup> However, accurate theories are still rare and polar molecules have proven particularly challenging to describe. According to the most elementary theories, such as the molecular Ammosov-Delone-Krainov theory (MO-ADK)<sup>14</sup> or the strong-field approximation (SFA),<sup>15</sup> the tunneling ionization

rate of a molecule is expected to maximize when the electron is removed via the location of maximal density of the highest-occupied molecular orbital (HOMO). Improvements over these basic theories must take into account the modification of the ionization potential by the Stark effect. This is crucial for the methyl halides which all have large permanent dipole moments ( $\text{CH}_3\text{F}$  : 1.85D,  $\text{CH}_3\text{Cl}$  : 1.87D,  $\text{CH}_3\text{Br}$  : 1.81D,  $\text{CH}_3\text{I}$  : 1.62D).<sup>16</sup> In addition, particular attention must be paid to the accuracy of the asymptotic part of the orbital wave functions which is crucial for obtaining accurate ionization rates. Finally, parabolic coordinates naturally provide a more accurate description of strong-field ionization in the tunneling limit because of the near-separability of coordinates. These essential developments have been implemented in the weak-field asymptotic theory (WFAT).<sup>17-20</sup> Other methods that have proven successful in describing strong-field ionization (SFI) of polar molecules include time-dependent multi-electron methods<sup>21-25</sup> but the predictive power of all theories largely remains to be established.

The challenge posed by SFI of polar molecules is well illustrated by the example of the carbonyl sulfide (OCS) molecule. This molecule has been examined by several research groups using different methods.<sup>26-31</sup> According to the most elementary theories, the SFI rate is expected to be largest when the electron is removed via the S atom where the density of the HOMO is maximal. However, Holmegaard *et al.*<sup>26</sup> showed experimentally that for circularly polarized laser pulses with a peak intensity of  $\approx 2.4 \times 10^{14}$  W/cm<sup>2</sup> the ionization of OCS is enhanced when the field points from the O to the S atom. They showed that the discrepancy between the calculated and observed ionization asymmetries may be attributed to the neglected Stark shift of the ionization potential in MO-ADK theory. Recently Ohmura *et al.*<sup>31</sup> presented experimental results where OCS was ionized by linearly polarized phase-controlled two-color pulses with a peak intensity of  $5 \times 10^{13}$  W/cm<sup>2</sup>. The two-color experiment suggested that ionization is enhanced when the electron is removed via the S atom. This result agreed with the ionization asymmetry predicted by the WFAT.<sup>32</sup> The example of the OCS molecule illustrates the fact that the electron density of the HOMO and the associated

linear Stark effect act in general antagonistically on the asymmetry of SFI. As a consequence, the accurate calculation of SFI rates is a challenging unresolved task, especially when multi-electron effects are important.

In this paper we report measurements of the asymmetries of dissociative ionization and Coulomb explosion of the methyl halides ( $\text{CH}_3\text{X}$ , with  $\text{X} = \text{F}, \text{Cl}, \text{Br}, \text{I}$ ) in phase-controlled two-color laser fields. We measure the angle-resolved momentum distribution spectra of different charged fragments as a function of the two-color phase. The measurements were repeated for multiple laser intensities. Further we have calculated the orientation-dependent ionization rates of the methyl halides based on the WFAT and compare its prediction with the experimental observations. We compare the results of the single-active-electron version of the WFAT, where dipole moments are calculated as expectation values over field-free orbitals, with an improved version that uses dipole moments calculated with multi-electron quantum chemical methods with applied static electric fields. We show that only the latter version agrees with the experimental results. Strong-field ionization of methyl halides in a phase-controlled two-color field has previously been measured by Ohmura<sup>33</sup> but was restricted to time-of-flight detection and a single laser intensity. Our results confirm their basic observations but show the presence of multiple dissociative ionization and Coulomb explosion channels. Most importantly, we show that the asymmetry of a given fragment can reverse as a function of the kinetic energy release and intensity. The former observation has previously been made in two-color experiments on apolar molecules<sup>34-36</sup> but not with polar molecules.<sup>31,37-39</sup> It shows the necessity of performing measurements with sufficient momentum resolution to identify multiple channels and to repeat measurements with multiple intensities to reveal the complexity of SFI of polar molecules. Our results additionally serve as a benchmark for theories of molecular SFI and highlight the importance of multi-electron effects in the Stark shifts.

# Experiment

The experiment was carried out using a velocity-map-imaging spectrometer (VMIS).<sup>40</sup> The two-color pulse was synthesized using second-harmonic generation in a  $\beta$ -barium-borate (BBO) crystal (300  $\mu\text{m}$  thickness). A 50-fs linearly polarized pulse with center wavelength of 800 nm passed through the crystal leading to the generation of an additional 400-nm pulse with polarization orthogonal to the incident beam. The 400-nm component had a spectral bandwidth of 6 nm, corresponding to a Fourier limit of 38 fs. A zeroth-order half-wave plate (at 800 nm) placed behind the crystal rotated the polarization plane of the 800-nm pulse by  $90^\circ$  to lie in the polarization plane of the 400-nm pulse. The intensity of the two-color pulse was adjusted by an iris placed directly in front of the entrance window (sapphire, 2.6 mm thickness) of the VMIS. The aperture diameter of the iris was varied between 1.8 mm and 2.6 mm. A spherical mirror ( $f = 100$  mm) mounted inside the VMIS focused the beam backwards into the center of the supersonic gas jet. The latter was formed by a pulsed Even-Lavie valve (orifice 150  $\mu\text{m}$ , 1 kHz repetition rate). Measurements were performed with  $\text{CH}_3\text{F}$ ,  $\text{CH}_3\text{Cl}$ ,  $\text{CH}_3\text{Br}$  and  $\text{CH}_3\text{I}$ . All target molecules were diluted in helium to a concentration of  $\leq 1\%$  to minimize clustering and space-charge effects. The group-delay dispersion of the BBO, the half-wave plate and the entrance window were compensated by a calcite plate (2.6 mm thickness) and two UV fused silica plates (total thickness of 2.5 mm). One UV fused silica plate (1.5 mm thickness) was mounted on a motorized rotation stage (Newport PR50PP). By tilting this plate, the relative phase  $\phi$  between the  $\omega$  and  $2\omega$  fields was adjusted. The intensity of the 400-nm pulse was  $(22\pm 3)\%$  of the total intensity for the used range of iris aperture diameters. To obtain the momentum-distribution spectra the measured VMIS images were Abel inverted using an iterative inversion method<sup>41</sup> (see Fig. 1). The inversion can lead to negative numbers especially for momenta where the signal is close to zero or which are close to the symmetry axis of the spectrum. These momenta were excluded from further analysis. The spectra were then convoluted with a Gaussian filter to reduce the high-frequency noise caused by the inversion. The full width at half maximum

of the filter function was 1% of the momentum detection range. The relative phase  $\phi$  of the two-color field defined as  $E(t) = E_1(t) \cos(\omega t) + E_2(t) \cos(2\omega t + \phi)$  was calibrated by measuring the dissociative ionization of CO.<sup>37</sup>

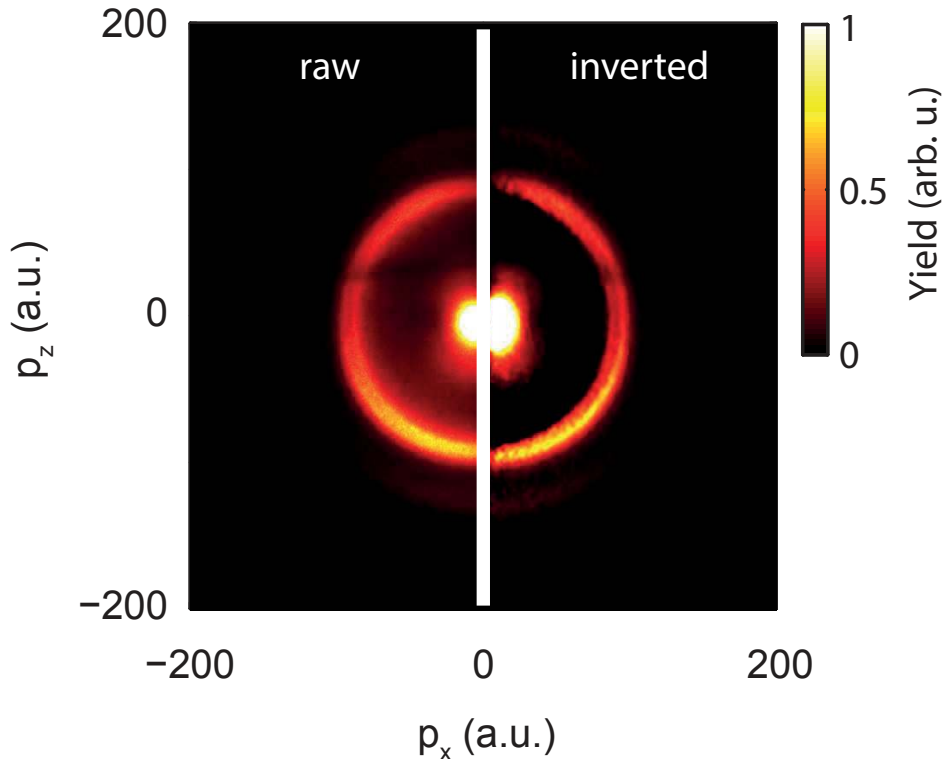


Figure 1: Raw and inverted images of  $\text{CH}_3^+$  from the interaction of  $\text{CH}_3\text{I}$  with an intense femtosecond 800+400-nm laser pulse (a. u. = atomic units). The direction of polarization of the two-color laser field was parallel to  $p_z$ .

## Results

The left panels of Figs. 2a-d show the yield spectra of the  $\text{CH}_3^+$  fragments from  $\text{CH}_3\text{X}$  (where X = F, Cl, Br and I) as a function of the kinetic energy. The  $\text{CH}_3^+$  ions can arise through the fragmentation of the parent ion following the reaction



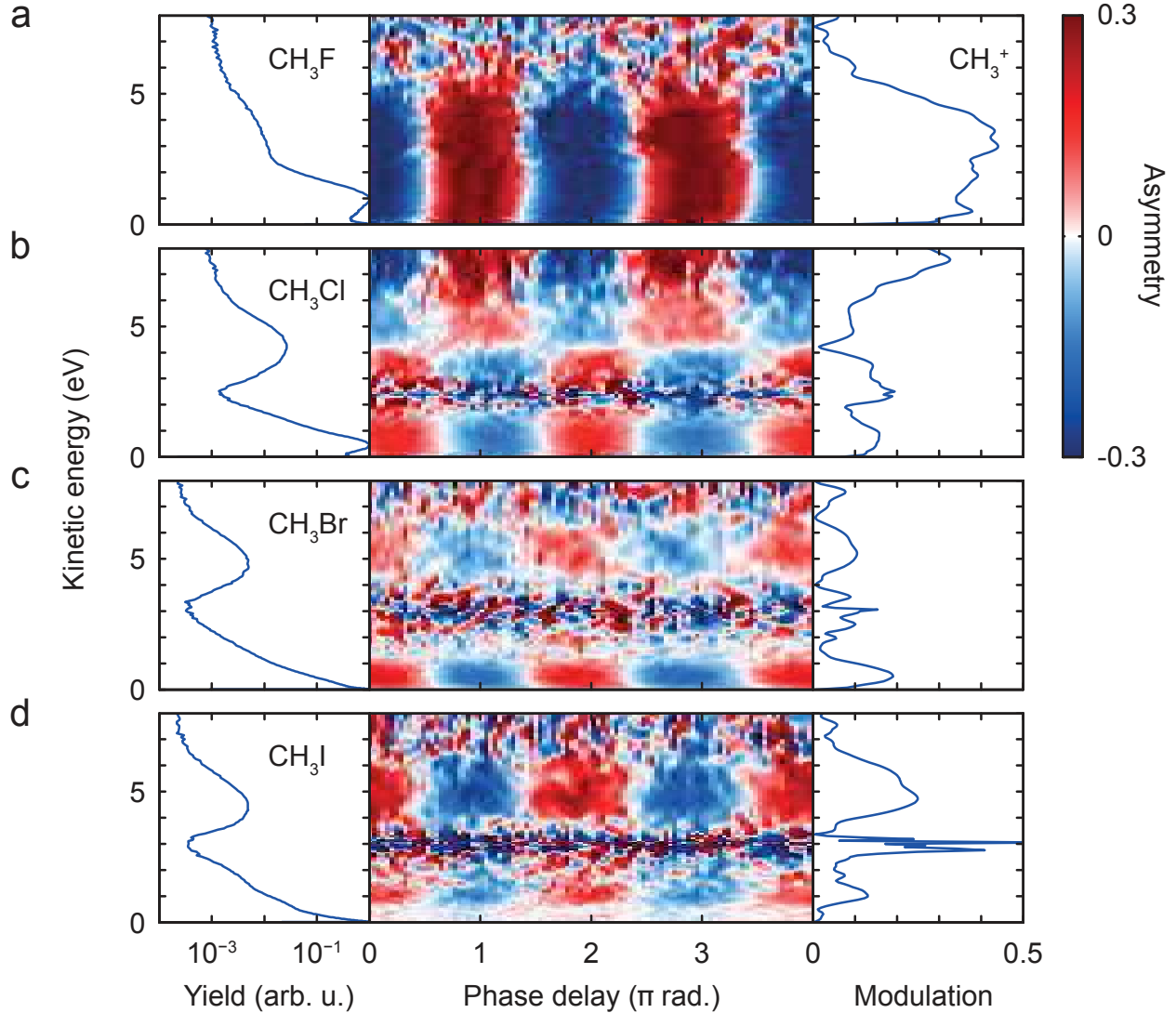


Figure 2: **Asymmetry of  $\text{CH}_3^+$  emission from methyl halides exposed to an intense two-color field.** (a) Spectrum of the normalized yield (left panel), density plot of the asymmetry  $\alpha$  defined in Eq. (4) (center panel) and modulation amplitude (right panel) of  $\text{CH}_3^+$  fragments from  $\text{CH}_3\text{F}$ . The laser peak intensity was  $(1.0 \pm 0.4) \times 10^{14} \text{ W/cm}^2$ . (b, c, d) Similar to (a) but from  $\text{CH}_3\text{Cl}$  (c),  $\text{CH}_3\text{Br}$  exposed to a laser peak intensity of  $(5 \pm 2) \times 10^{13} \text{ W/cm}^2$  (d),  $\text{CH}_3\text{I}$ , exposed to a laser peak intensity of  $(3 \pm 1) \times 10^{13} \text{ W/cm}^2$ .

where  $q = 0, 1, \dots$  and  $X = \text{F, Cl, Br or I}$ . In the case of a two-body fragmentation process it is sufficient to know the energy of one fragment to obtain the center-of-mass energy. Therefore one can distinguish different dissociation channels based on the energy of the  $\text{CH}_3^+$  ions alone. In all spectra local maxima or shoulders near 0 eV and 3-5 eV can be observed. The peak near 5 eV in the yield spectrum of  $\text{CH}_3\text{I}$  is assigned to the Coulomb explosion of



the doubly charged parent ion to  $\text{CH}_3^+$  and  $\text{I}^+$ .<sup>42</sup> The peak near 0 eV is attributed to the dissociative ionization of  $\text{CH}_3\text{I}$  into  $\text{CH}_3^+$  and  $\text{I}$ .<sup>43</sup> Since the yield spectra of all four molecules are very similar, this assignment is most likely also valid for the other three methyl halides. This assignment was confirmed by calculating the kinetic energy of  $\text{CH}_3^+$  resulting from the Coulomb explosion of the doubly charged parent ions using either the purely Coulombic repulsion energy or a high-level ab-initio calculation. We first discuss the simple Coulomb model and then describe the ab-initio calculations.

*Coulomb Model* : The purely Coulombic part of the kinetic energy release ( $E_{\text{CM}}^{\text{C}}$  in Tables I-III) was calculated by assuming two point charges  $Q_1 = pe$  and  $Q_2 = qe$  to be separated by a distance  $R$  between the centers of mass of the fragments, i.e.

$$E_{\text{CM}}^{\text{C}} = \frac{pqe^2}{4\pi\epsilon_0 R} \quad (2)$$

where  $e$  is the elementary charge and  $\epsilon_0$  the permittivity of vacuum. The kinetic energy of a single fragment from a two-body dissociation is

$$E_{\text{frag}} = \frac{m_{\text{mol}} - m_{\text{frag}}}{m_{\text{mol}}} E_{\text{CM}} \quad (3)$$

where  $m_{\text{mol}}$  and  $m_{\text{frag}}$  represent the total mass of the molecule and the mass of the fragment, respectively. The results for the Coulomb explosion leading to  $\text{CH}_3^+ + \text{X}^+$  are summarized in Table 1. The kinetic energy  $E_{\text{CH}_3^+}^{\text{C}}$  was obtained by choosing  $R = R_{\text{CX}}$  where  $R_{\text{CX}}$  represents the distance between the halogen atom and the center of mass of the methyl group. The center-of-mass energy  $E_{\text{CM}}^{\text{C}}$  decreases from  $\text{CH}_3\text{F}$  to  $\text{CH}_3\text{I}$ , however the kinetic energy  $E_{\text{CH}_3^+}^{\text{C}}$  of the  $\text{CH}_3^+$  fragments lies between 5.4 eV and 6.1 eV for all molecules. The obtained energies are systematically higher than the positions of the observed peaks in the kinetic-energy spectra.

*Ab-initio calculations* : Much more accurate values for the kinetic-energy release were obtained from ab-initio quantum chemical calculations. We used the CCSD(T) method with

the cc-pVQZ and cc-pV5Z all-electron basis sets for X = F, Cl, Br and corresponding pseudo-potential basis sets for X = Br and I. Electronic energies were extrapolated to the complete basis set limit. Relativistic effects have been estimated with the 2<sup>nd</sup>-order Douglas-Kroll-Hess (DKH2) and 4<sup>th</sup>-order Douglas-Kroll-Hess (DKHSO) approximations using the cc-pV5Z-DK basis sets for all electron calculations for X = F, Cl and Br. These calculations reproduced the second ionization potentials of F, Cl, Br and I within 0.4 eV. The kinetic-energy releases were calculated using MP2/cc-pVTZ-optimized geometries for CH<sub>3</sub>X, CX<sup>+</sup>, CX<sup>2+</sup>, CH<sub>3</sub><sup>+</sup> and H<sub>3</sub><sup>+</sup> assuming vertical ionization of the CH<sub>3</sub>X molecule followed by dissociation to the equilibrium geometry of the fragments in their electronic ground state which are the following: CH<sub>3</sub>X<sup>2+</sup> (<sup>3</sup>A<sub>1</sub>, C<sub>3v</sub> symmetry), CH<sub>3</sub>X<sup>3+</sup> (<sup>2</sup>E, C<sub>3v</sub> symmetry), CH<sub>3</sub><sup>+</sup> (<sup>1</sup>A<sub>1</sub>, D<sub>3h</sub> symmetry), H<sub>3</sub><sup>+</sup> (<sup>1</sup>A<sub>1</sub>, D<sub>3h</sub> symmetry), CX<sup>+</sup> (<sup>1</sup>Σ<sub>g</sub><sup>+</sup>), CX<sup>2+</sup> (<sup>2</sup>Σ<sub>g</sub><sup>+</sup>), X<sup>+</sup> (<sup>3</sup>P), X<sup>2+</sup> (<sup>4</sup>S). Total predicted kinetic-energy releases ( $E_{\text{CM}}^{\text{ai}}$  in Tables I-III) were obtained from basis set extrapolated electronic energies and including zero-point vibrational energies estimated from MP2/cc-pVTZ harmonic frequencies of the molecular fragments. Remaining basis set errors are likely to be less than 0.1 eV for the all-electron results whereas the pseudo-potential approximation appears to have errors around 0.2 eV for the triply-charged species. Based on the MP2, CCSD and CCSD(T) results, remaining errors in the electronic correlation energies are likely to lie below 0.2-0.3 eV. The estimated errors in the zero-point vibrational energies are in the range of 0.01 eV.

*Comparison between Coulomb and ab-initio calculations* : The kinetic energy releases  $E_{\text{CM}}^{\text{ai}}$  calculated ab-initio systematically lie below the purely Coulombic repulsion energies  $E_{\text{CM}}^{\text{C}}$  as a consequence of a large covalent bonding character of the electronic ground states of the doubly and triply charged methyl-halide molecules. Since the electronic ground states of these species usually have the highest covalent bond strengths,  $E_{\text{CM}}^{\text{ai}}$  can be considered to represent the lower limit of kinetic energy release from a given charge state. The kinetic energy releases from electronically-excited states will in general be higher than  $E_{\text{CM}}^{\text{ai}}$  and can even lie above  $E_{\text{CM}}^{\text{C}}$  when an electronic state with a repulsive covalent character is accessed.

These results allow us to identify the local maxima between 3 and 7 eV in the  $\text{CH}_3^+$  spectra of Figs. 2b-d, as well as the broad shoulder between 3 and 5 eV in Fig. 2a, with  $\text{CH}_3^+$  from the Coulomb explosion of  $\text{CH}_3\text{X}^{2+}$ . This assignment also agrees with the results of Ref.<sup>42</sup> on  $\text{CH}_3\text{I}^{2+}$ .

**Table 1:** Calculated kinetic-energy release (in eV) for the dissociation reaction  $\text{CH}_3\text{X}^{2+} \rightarrow \text{CH}_3^+ + \text{X}^+$  based on the purely Coulombic energies (Eq. (2)) or an ab-initio calculation described in the text. Both the total center-of-mass energy  $E_{\text{CM}}$  of the two fragment ions and the kinetic energy  $E_{\text{CH}_3^+}$  of the  $\text{CH}_3^+$  fragments are given. The internuclear distance between the halogen atom  $\text{X}$  and methyl group  $\text{CH}_3$  -  $R_{\text{CX}}$  (Å) used in the calculations and the experimental kinetic energy (KE) peak are given.

	$R_{\text{CX}}$	Coulomb		ab-initio		Our Expt.
		$E_{\text{CM}}^{\text{C}}$	$E_{\text{CH}_3^+}^{\text{C}}$	$E_{\text{CM}}^{\text{ai}}$	$E_{\text{CH}_3^+}^{\text{ai}}$	
$\text{CH}_3\text{F}$	1.46	9.9	5.5	4.2	2.3	3.4
$\text{CH}_3^{35}\text{Cl}$	1.86	7.7	5.4	5.0	3.5	4.3
$\text{CH}_3^{79}\text{Br}$	2.00	7.2	6.1	4.7	4.0	5.1
$\text{CH}_3\text{I}$	2.20	6.5	5.9	3.8	3.4	4.7

*Asymmetry of  $\text{CH}_3^+$  from  $\text{CH}_3\text{X}$ :* The measured emission asymmetry of  $\text{CH}_3^+$  as a function of the kinetic energy and the two-color phase  $\phi$  is shown on the right-hand side of Figs. 2a-d. The asymmetry  $\alpha(E, \phi)$  as a function of the kinetic energy  $E$  and the two-color phase  $\phi$  is defined as

$$\alpha(E, \phi) = \frac{Y_{\text{up}}(E, \phi) - Y_{\text{down}}(E, \phi)}{Y_{\text{up}}(E, \phi) + Y_{\text{down}}(E, \phi)} \quad (4)$$

where  $Y_{\text{up}}(E, \phi)$  and  $Y_{\text{down}}(E, \phi)$  are the ion yields collected in the upper or lower hemisphere along the direction of the polarization axis, respectively. At  $\phi = 0$  the maximal amplitude of the asymmetric two-color field points in the direction called "up". For  $\text{CH}_3\text{F}$  (Fig. 2a) the asymmetry  $\alpha(E, \phi)$  at  $\phi = 0$  is negative over the complete energy range. Moreover, the asymmetry modulates in phase with respect to  $\phi$ . The amplitude of the modulation as a function of the kinetic energy is shown on the right-hand side of the density plot. In the case of  $\text{CH}_3\text{F}$  amplitudes of up to 0.44 were observed. From the emission asymmetry of  $\text{CH}_3^+$  from  $\text{CH}_3\text{F}$  one can conclude that both the dissociative ionization ( $q = 0$  in reaction

(1)) and Coulomb explosion ( $q = 1$ ) are faster when the maximal electric field vector points from the methyl group to the fluorine atom, i.e. the electron is removed via the methyl group. For  $\text{CH}_3^+$  emitted from  $\text{CH}_3\text{Cl}$ ,  $\text{CH}_3\text{Br}$  and  $\text{CH}_3\text{I}$  in contrast, a positive asymmetry of fragments with energies  $< 4$  eV was observed for  $\phi = 0$  (Figs. 2b-c). It follows that the dissociative ionization and Coulomb explosion generating the lowest-energy fragments of these molecules are enhanced when the electric field maximum points from the halogen atom to the methyl group, i.e. in the opposite direction compared to  $\text{CH}_3\text{F}$ . However, in the density plot of  $\text{CH}_3\text{Cl}$  (Fig. 2b) a clear change of the asymmetry can be observed at 4.2 eV. The  $\text{CH}_3^+$  fragments with kinetic energies larger than 4.2 eV must therefore originate from a different channel than those with a smaller kinetic energy. The change in asymmetry occurs at the maximum of the peak assigned to the  $\text{CH}_3\text{Cl}^{2+} \rightarrow \text{CH}_3^+ + \text{Cl}^+$  reaction. As we further discuss below, the reversal in the asymmetry is likely to originate from ionization to electronically-excited states of  $\text{CH}_3\text{Cl}^{2+}$ , e.g. by removing the first electron from HOMO and the second one from HOMO-1 or HOMO-2.

**Table 2:** Calculated kinetic-energy release (in eV) for the dissociation reaction  $\text{CH}_3\text{X}^{2+} \rightarrow \text{CX}^+ + \text{H}_3^+$  based on the purely Coulombic energies (Eq. (2)) or an ab-initio calculation described in the text. Both the total center-of-mass energy  $E_{\text{CM}}$  of the two fragment ions and the kinetic energy  $E_{\text{H}_3^+}$  of the  $\text{H}_3^+$  fragments are given.

	Coulomb		ab-initio	
	$E_{\text{CM}}^{\text{C}}$	$E_{\text{H}_3^+}^{\text{C}}$	$E_{\text{CM}}^{\text{ai}}$	$E_{\text{H}_3^+}^{\text{ai}}$
$\text{CH}_3^{35}\text{Cl}$	8.4	7.9	5.87	5.52
$\text{CH}_3^{79}\text{Br}$	7.2	6.9	4.02	3.89

*Formation and Asymmetry of  $\text{H}_3^+$*  : In addition to the previously observed dissociative ionization and Coulomb explosion channels, we have also observed the reaction



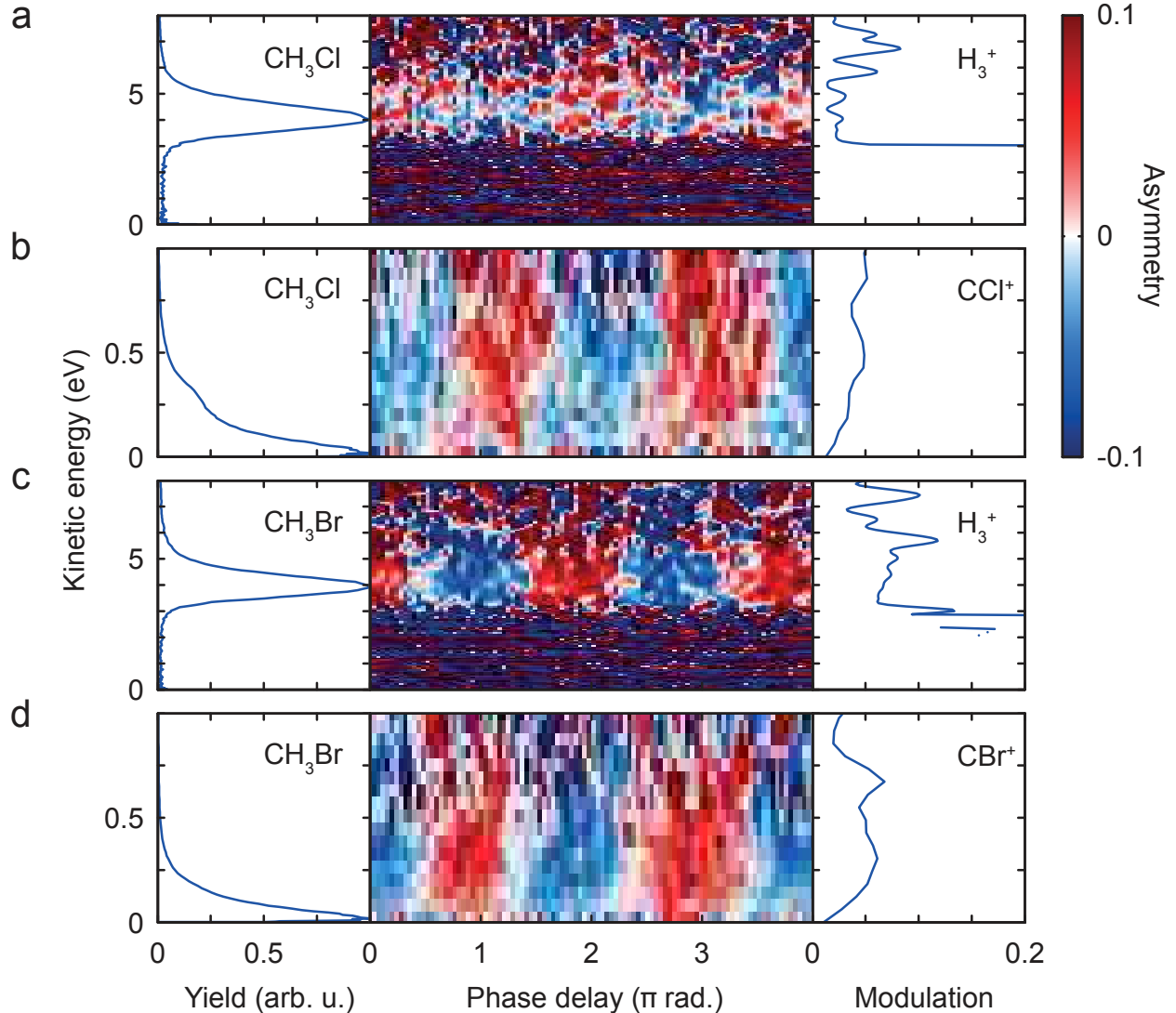


Figure 3: **Dissociative ionization leading to the formation of  $\text{H}_3^+$** . Similar to Fig. 2, but for  $\text{H}_3^+$  (a) and  $\text{CCl}^+$  (b) from  $\text{CH}_3\text{Cl}$  and  $\text{H}_3^+$  (c) and  $\text{CBr}^+$  (d) from  $\text{CH}_3\text{Br}$ . The laser peak intensity was  $(1.6 \pm 0.6) \times 10^{14} \text{ W/cm}^2$ .

leading to the formation of  $\text{H}_3^+$ . This reaction is particularly interesting because it requires the breaking and formation of three bonds.<sup>44,45</sup> The measured asymmetries of  $\text{H}_3^+$  and  $\text{CX}^+$  from  $\text{CH}_3\text{Cl}$  and  $\text{CH}_3\text{Br}$  are given in Figs. 3a-d, respectively. At  $\phi = 0$  the asymmetry is positive for  $\text{H}_3^+$  from  $\text{CH}_3\text{Cl}$  and  $\text{CH}_3\text{Br}$ , identical to the asymmetry of the low-energy  $\text{CH}_3^+$  fragments from the corresponding molecules. As expected, the asymmetry of the  $\text{CX}^+$  fragments is opposite to the asymmetry of the  $\text{H}_3^+$  ions. Sun *et al.*<sup>44</sup> studied the formation of  $\text{H}_3^+$  from  $\text{CH}_3\text{Cl}$  in a symmetric femtosecond laser field and reported a maximum of the  $\text{H}_3^+$

yield at a kinetic energy of 1.69 eV whereas we measured an energy of 4.0 eV. The reported laser peak intensity in Ref. <sup>44</sup> was  $9.4 \times 10^{13} \text{ W/cm}^2$ , not sufficiently different from the peak intensity used in our study ( $(1.6 \pm 0.6) \times 10^{14} \text{ W/cm}^2$ ) to explain the large difference in kinetic energies. Our experimental value is also closer to the predicted kinetic energy  $E_{\text{H}_3^+}^{\text{ai}}$  of the  $\text{H}_3^+$  fragments given in Table 2.

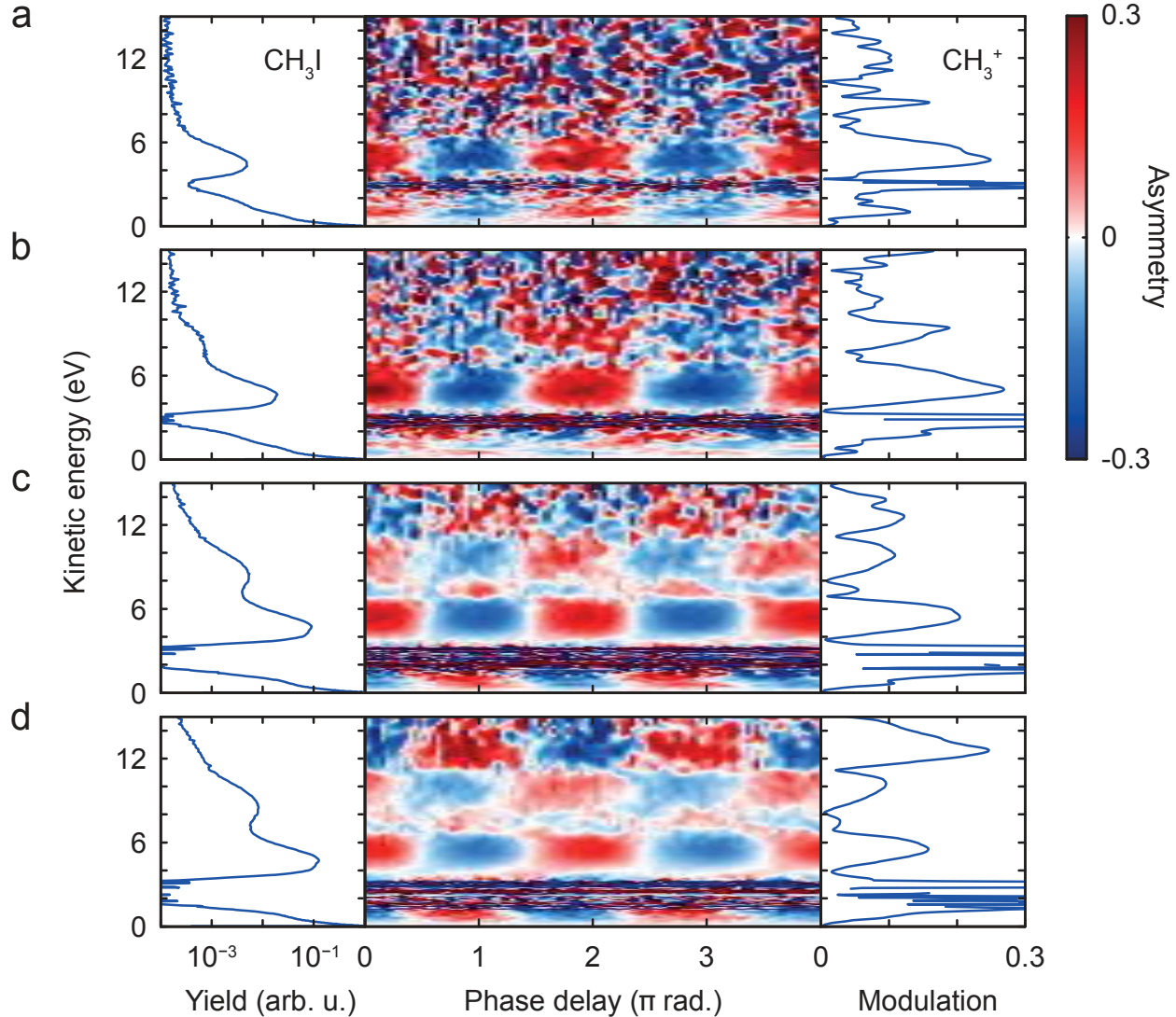


Figure 4: **Intensity dependence of the dissociation asymmetry of  $\text{CH}_3^+$  from  $\text{CH}_3\text{I}$ .** The laser peak intensity was  $(3 \pm 1) \times 10^{13} \text{ W/cm}^2$  (a),  $(5 \pm 2) \times 10^{13} \text{ W/cm}^2$  (b),  $(1 \pm 0.4) \times 10^{14} \text{ W/cm}^2$  (c) and  $(1.6 \pm 0.6) \times 10^{14} \text{ W/cm}^2$  (d).

*Asymmetry of  $\text{CH}_3^+$  and  $\text{I}^+$  from  $\text{CH}_3\text{I}$ :* We now show that the relatively simple results

displayed in Fig. 2 become significantly more complex at higher intensities of the two-color probe field. Here, we will mainly focus on the results obtained for  $\text{CH}_3\text{I}$ , although similar observations have also been made for  $\text{CH}_3\text{Cl}$  and  $\text{CH}_3\text{Br}$ . The effect of the laser intensity on the yield spectrum and the asymmetry of  $\text{CH}_3^+$  from  $\text{CH}_3\text{I}$  is shown in Figs. 4a-d. The measured abundance ratio is  $\text{I}^+:\text{I}^{2+}:\text{I}^{3+}:\text{I}^{4+} = 1 : 0.47 : 0.10 : 0.01$  at the intensity  $1 \times 10^{14} \text{Wcm}^{-2}$  (panel c). The yield of high-kinetic-energy fragments is found to increase as a function of intensity with the appearance of additional maxima. The evolution of the asymmetry reveals two main changes as a function of intensity. First, the emission asymmetry of the peak near 0 eV changes sign with increasing intensity. This shows that the asymmetry of the dissociative-ionization channel producing  $\text{CH}_3^+ + \text{I}$  with very small kinetic energies changes sign as a function of intensity. The second change is the appearance of high-energy  $\text{CH}_3^+$  fragments which have the opposite asymmetry compared to the fragments observed in Fig. 2d. Clear reversals of the sign of the asymmetry are observed at 6.9 eV, 8.0 eV and 11.2 eV in Figs. 4c-d. Deviations between the asymmetry maxima in different panels are small and within the experimental uncertainty. We note that this observation stands in contrast to results that we have obtained on  $\text{CH}_3\text{Cl}$  (not shown), where asymmetry features display continuous transitions in their phase dependence, which suggests the presence of multiple overlapping channels.

The relation between the energy  $E_{\text{CH}_3^+}$  of  $\text{CH}_3^+$  ions and the energy  $E_{\text{I}^{q+}}$  of  $\text{I}^{q+}$  ions from Coulomb explosion according to eq. (1) is given by

$$\frac{E_{\text{I}^{q+}}}{E_{\text{CH}_3^+}} = \frac{m_{\text{CH}_3^+}}{m_{\text{I}^{q+}}} \quad (6)$$

where  $m_{\text{CH}_3^+}$  and  $m_{\text{I}^{q+}}$  are the masses of the fragments. The predicted kinetic energies for  $\text{CH}_3^+$  and  $\text{I}^{q+}$  fragments calculated using equations (2) and (3) are given in Table 3 for  $q = 1 - 4$ . In addition, we also report the corresponding values obtained from the ab-initio calculations described above. Based on the relation (6) and together with the emission

asymmetry it is thus possible to find correlations between measurements of the  $\text{CH}_3^+$  and  $\text{I}^{q+}$  ions. We identify the kinetic energies of  $\text{CH}_3^+$  fragments corresponding to 4.7 eV, 7.4 eV, 9.8 eV and 12.6 eV - where we see strongly modulating yield (see Fig. 4c) and discuss the correlations with  $\text{I}^{q+}$ . These fragment kinetic energies correspond to a total kinetic-energy release (KER) of 5.3 eV, 8.3 eV, 11 eV and 14 eV, respectively. The emission asymmetries of the different ions are compared in Fig. 5 - (a)  $\text{CH}_3^+$  (b)  $\text{I}^+$  (c)  $\text{I}^{2+}$  (d)  $\text{I}^{3+}$  (e)  $\text{I}^{4+}$ . The KER distribution is plotted on the left for comparison. The horizontal green lines are drawn at the above mentioned KER values. The comparison and correlation between fragments based on KER is only valid for two-body dissociation channels.

**Table 3: Calculated kinetic-energy release (in eV) for the dissociation reaction  $\text{CH}_3\text{I}^{(1+q)+} \rightarrow \text{CH}_3^+ + \text{I}^{q+}$  based on the purely Coulombic energies (Eq. (2)) or an ab-initio calculation described in the text. Both the total center-of-mass energy  $E_{\text{CM}}$  of the two fragment ions and the kinetic energy  $E_{\text{CH}_3^+}$  of the  $\text{CH}_3^+$  fragments are given.**

$q$	Coulomb			ab-initio		
	$E_{\text{CM}}^{\text{C}}$	$E_{\text{CH}_3^+}^{\text{C}}$	$E_{\text{I}^{q+}}^{\text{C}}$	$E_{\text{CM}}^{\text{ai}}$	$E_{\text{CH}_3^+}^{\text{ai}}$	$E_{\text{I}^{q+}}^{\text{ai}}$
1	6.5	5.9	0.7	3.8	3.4	0.4
2	13.1	11.7	1.4	11.3	10.1	1.2
3	19.6	17.6	2.1	14.3	12.8	1.5
4	26.2	23.4	2.8	17.4	15.6	1.8

- *KER 5.3 eV* : This KER corresponds to fragment kinetic energies of 4.7 eV and 0.6 eV for  $\text{CH}_3^+$  and  $\text{I}^{q+}$ , respectively. Following the horizontal green line at 5.3 eV in Figs. 5 (a) and (b), one finds opposite emission asymmetry for  $\text{CH}_3^+$  and  $\text{I}^+$  at this energy, as expected for a two-body fragmentation pathway. This KER lies between the  $E_{\text{CH}_3^+}$  obtained from Coulomb and ab-initio calculations in Table III ( $q = 1$ ). We therefore assign the fragmentation channel to be  $\text{CH}_3\text{I}^{2+} \rightarrow \text{CH}_3^+ + \text{I}^+$ .
- *KER 8.3 eV* : The individual kinetic energies of  $\text{CH}_3^+$  and  $\text{I}^{q+}$  are 7.4 eV and 0.9 eV, respectively in a two-body fragmentation scheme. Following the horizontal green line at 8.3 eV, from panel (a) to (b) does not show the expected reversal of asymmetry.



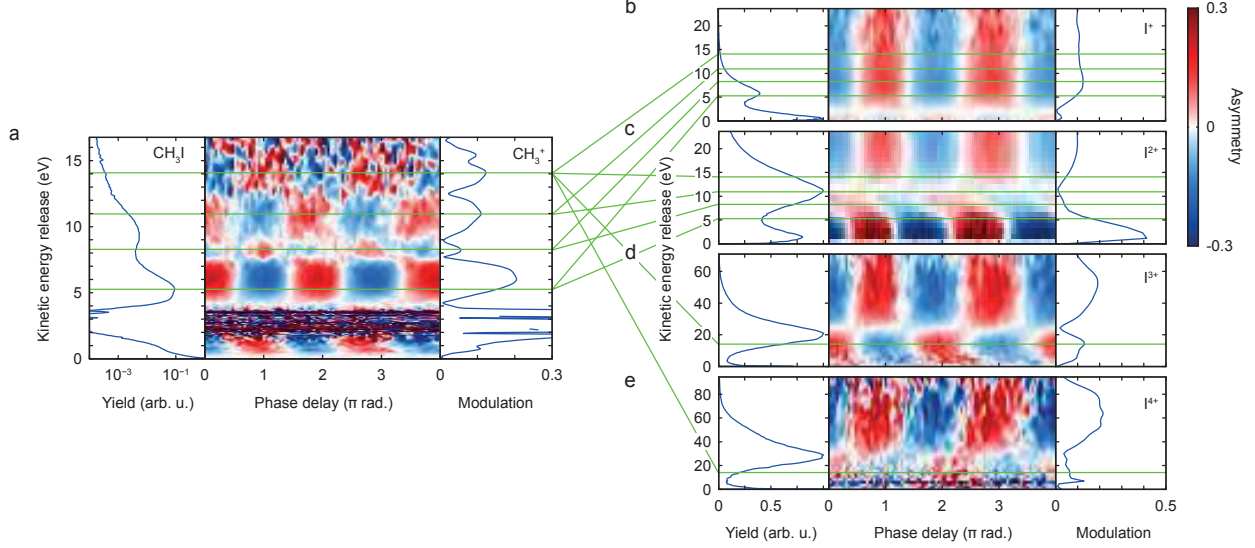


Figure 5: **Correlation between different fragments from  $\text{CH}_3\text{I}$**  - (a)  $\text{CH}_3^+$ , (b)  $\text{I}^+$ , (c)  $\text{I}^{2+}$ , (d)  $\text{I}^{3+}$  and (e)  $\text{I}^{4+}$ . The laser peak intensity was  $(1 \pm 0.4) \times 10^{14} \text{ W/cm}^2$ . The measured abundance ratio of  $\text{I}^+ : \text{I}^{2+} : \text{I}^{3+} : \text{I}^{4+}$  is  $1 : 0.47 : 0.10 : 0.01$ . The green lines in (a), (b) and (c) are plotted at KER values of 5.3 eV, 8.3 eV, 11 eV and 14 eV corresponding to local maxima in the modulation of the asymmetry yield whereas the one in (d) and (e) corresponds to 14 eV.

However, the asymmetry plot of  $\text{I}^{2+}$  (c) does reveal the expected opposite asymmetry. Comparison with Coulomb and ab-initio calculations for  $q = 2$  in Table III however shows that the KER is at least 2.7 eV smaller than expected for the  $\text{CH}_3\text{I}^{3+} \rightarrow \text{CH}_3^+ + \text{I}^{2+}$  channel. Therefore, we exclude this assignment. We conclude that the  $\text{CH}_3^+$  fragments with kinetic energies close to 7.4 eV originate from a  $\text{CH}_3\text{I}^{2+} \rightarrow \text{CH}_3^+ + \text{I}^+$  channel which displays an asymmetry opposite to that of the dominant channel producing  $\text{CH}_3^+$  with a kinetic energy centered at 4.7 eV. Ionisation to electronically-excited states of  $\text{CH}_3\text{I}^{2+}$  by e.g. removing one electron from HOMO and one from HOMO-1 or HOMO-2, is a likely explanation. Since the asymmetry feature in  $\text{CH}_3^+$  is only  $\sim 1\text{eV}$  broad, the corresponding feature in the  $\text{I}^{q+}$  fragment spectrum would be 0.12 eV wide, well below the width of the Gaussian filter used to smooth the data. This fact, dissociation into more than two fragments or overlap with a dominant channel, may explain the absence of the expected asymmetry pattern in  $\text{I}^{2+}$ .

- *KER 11 eV* : The third horizontal line at 11 eV in panel (a) corresponds to  $\text{CH}_3^+$  and  $\text{I}^{q+}$  with 9.8 eV and 1.2 eV kinetic energy, respectively. There is a clear peak at 11 eV in panel (c) showing a very weak asymmetry in  $\text{I}^{2+}$ , which has the same rather than the opposite sign as  $\text{CH}_3^+$ . The asymmetry of  $\text{I}^{2+}$  (panel (c)) changes sign just above 11 eV. The observed asymmetry would also be compatible with that observed in  $\text{I}^+$  (panel (b)), possibly as a consequence of sequential ionization. However, the high kinetic energy is incompatible with this assignment (see Table III for  $q = 1$ ). Because of the close agreement with  $E_{\text{CH}_3^+}^{\text{ai}} = 10.1$  eV, we assign this channel to  $\text{CH}_3\text{I}^{3+} \rightarrow \text{CH}_3^+ + \text{I}^{2+}$ , despite the lack of agreement in the emission asymmetry of the two co-fragments.
- *KER 14 eV* : The horizontal green line at KER 14 eV corresponds to a kinetic energy of 12.6 eV for  $\text{CH}_3^+$  and 1.4 eV for  $\text{I}^{q+}$ . The asymmetry in ion yields is clearly opposite for  $\text{I}^{3+}$  in panel(d). The kinetic energy values match very well with ab-initio calculations for  $q = 3$  in Table III. We unambiguously assign this channel to  $\text{CH}_3\text{I}^{4+} \rightarrow \text{CH}_3^+ + \text{I}^{3+}$ .

## Discussion

The asymmetries observed in the present experiments can originate from multiple sources. Since the electronic ground state of all  $\text{CH}_3\text{X}^+$  molecules is strongly bound, single ionization from the HOMO will not lead to direct dissociation. However,  $\text{CH}_3\text{X}^+$  in its electronic ground state may dissociate following absorption of photons from the two-color pulse, including bond softening, or excitation by the re-colliding electron. These processes may result in asymmetric emission of low-energy charged fragments which is, however, not directly related to the asymmetry of the ionization process. Similarly, the electronic ground states of  $\text{CH}_3\text{X}^{2+}$  are bound and sufficiently long-lived to appear in the time-of-flight spectra (see also Refs.<sup>44,46</sup>). However, in contrast to  $\text{CH}_3\text{X}^+$ , the low barrier to Coulomb explosion ( $\approx 0.1$  eV in  $\text{CH}_3\text{I}^{2+}$ <sup>42</sup>)

and the pronounced shortening of the C-X bond upon double ionization from the anti-bonding HOMO will lead to direct dissociation of a large fraction of the molecules.

In addition to these mechanisms, ionization to electronically excited states of the cations can occur. Since the  $\tilde{A}^+$  state of all  $\text{CH}_3\text{X}^+$  molecules is weakly bound, a large fraction of molecules ionized out of HOMO-1 will dissociate directly. The same principle also applies to double ionization which can lead to electronically excited states of the di-cation, e.g. through ionization from HOMO and HOMO-1 or even more strongly bound orbitals.

The channel that offers the simplest interpretation with respect to the asymmetry of SFI is therefore the Coulomb explosion of the electronic ground state of  $\text{CH}_3\text{X}^{2+} \rightarrow \text{CH}_3^+ + \text{X}^+$ . This channel has been identified in all experiments in the range of  $\text{CH}_3^+$  kinetic energies of 3.5-5 eV. Methyl fragments with less than 4.2 eV kinetic energy show opposite emission asymmetries in the case of  $\text{CH}_3\text{F}$  compared to  $\text{CH}_3\text{Cl}$ ,  $\text{CH}_3\text{Br}$  or  $\text{CH}_3\text{I}$  (Figs. 2a-d). As we show now, this observation can be explained by the asymmetry of SFI under the assumption that both electrons are removed from the HOMO. The orientation-dependent ionization rates were calculated based on the WFAT.<sup>17,18</sup>

*WFAT Ionization rates* : In the WFAT the total ionization rate is given by

$$\Gamma = \sum_{n_\xi=0}^{\infty} \sum_{m=-\infty}^{\infty} \Gamma_{n_\xi m} + O(\Gamma^2) \quad (7)$$

where

$$\Gamma_{n_\xi m} = |G_{n_\xi m}(\beta, \gamma)|^2 W_{n_\xi m}(F)[1 + O(F)] \quad (8)$$

is the partial rate for ionization into a channel with parabolic quantum numbers  $n_\xi$  and  $m$ . In the leading-order approximation of the asymptotic expansion in field  $F$  the ionization rate is determined by the dominant ionization channel with  $n_\xi = m = 0$  and given by

$$\Gamma(\beta, \gamma) \approx \Gamma_{00} = |G_{00}(\beta, \gamma)|^2 W_{00}(F)[1 + O(F)], \quad (9)$$

where  $W_{00}(F)$  is the field factor, an exponential function of the external field  $F$ .<sup>17</sup> The orientation dependence of  $\Gamma(\beta, \gamma)$  in this approximation thus does not depend on the field strength and is fully described by the structure factor  $G_{00}(\beta, \gamma)$ , where  $\beta$  and  $\gamma$  represent the Euler angles. The angle  $\beta$  is defined such that for  $\beta = 0^\circ$  the electron is removed from the methyl side. The normalized values of the squared structure factor  $|G_{00}(\beta, \gamma)|^2$  integrated over the angle  $\gamma$  are shown in Fig. 6. The green and blue lines represent the results obtained for the two eigenfunctions  $\Psi_A$  and  $\Psi_B$  of the HOMO in a quasi-static electric field, respectively. These eigenfunctions are orientation-dependent linear combinations of the field-free orbitals  $\phi_a$  and  $\phi_b$ ,<sup>47</sup> i.e.

$$\begin{aligned}\Psi_A &= (-S\phi_a + C\phi_b) \operatorname{sgn} C \\ \Psi_B &= (+C\phi_a + S\phi_b) \operatorname{sgn} S\end{aligned}\tag{10}$$

where  $S = \sin(\gamma/2 + \pi/4)$  and  $C = \cos(\gamma/2 + \pi/4)$ . The corresponding eigenvalues

$$z_{A/B} = (\mp U \sin \beta - V \cos \beta)\tag{11}$$

include the coupling constants  $U$  and  $V$  representing the linear Stark effect. The structure factor  $G_{00}(\beta, \gamma)$  is obtained as explained in Ref.<sup>47</sup> using Hartree-Fock calculations. We use uncontracted polarization-consistent basis sets on the quintuple zeta (pc-4) quality level and variationally optimize all exponents of the basis set. Because the HOMO of the methyl halides has a nodal plane containing the CX bond,  $|G_{00}(\beta, \gamma)|^2$  is zero for  $\beta = 0^\circ$  and  $\beta = 180^\circ$ . We now define the head-to-tail ionization asymmetry  $a$  as

$$\begin{aligned}a &= \left( \int_0^{\pi/2} \int_0^{2\pi} \Gamma(\beta, \gamma) \sin(\beta) d\beta d\gamma \right. \\ &\quad \left. - \int_{\pi/2}^{\pi} \int_0^{2\pi} \Gamma(\beta, \gamma) \sin(\beta) d\beta d\gamma \right) \\ &\quad / \int_0^{\pi} \int_0^{2\pi} \Gamma(\beta, \gamma) \sin(\beta) d\beta d\gamma.\end{aligned}\tag{12}$$

The ionization asymmetries  $a$  for the two eigenfunctions of the HOMO are given in Table 4 and Fig. 6. For  $a > 0$  the molecule preferentially ionizes from the methyl end. In this article we compare results of the single-active-electron version of the WFAT<sup>17,18</sup> where  $U$  and  $V$  are obtained as expectation values over  $\phi_a$  and  $\phi_b$  which yields the asymmetries  $a'$  with results where  $U$  and  $V$  were obtained from multi-electron quantum-chemical calculations with applied static electric fields yielding the asymmetries  $a$ . In more detail, the Stark shift of the binding energies was calculated on the HF/aug-cc-pVQZ level of theory for CH<sub>3</sub>F, CH<sub>3</sub>Cl and CH<sub>3</sub>Br and the HF/6-311G\*\* level for CH<sub>3</sub>I. The binding energies of the two components of the degenerate HOMO and HOMO-2 were calculated in the presence of static fields up to 0.05 a.u. and a second-order polynomial fit was used to extract the coefficients of the linear Stark effect. The  $U$  and  $V$  coefficients were determined by applying static fields along the three principal axes of the molecule and averaging over fields applied along  $\pm z$  (V) or  $\pm x$  and  $\pm y$  (U). This approach includes multi-electron effects into the treatment of the Stark effect and is consistent with the many-electron WFAT developed in Ref.<sup>48</sup> In the case of the non-degenerate HOMO-1 ( $a_1$  symmetry)  $U = 0$  by symmetry and  $V$  is obtained as described above. The HOMO-2 of all CH<sub>3</sub>X molecules are degenerate ( $e$  symmetry) and were treated in the same way as the HOMO. All ionization-rate asymmetries provided by the WFAT are independent of the field strength within the leading-order approximation used in the present work.

**Table 4: Head-to-tail ionization asymmetries  $a'$  calculated within the single-active-electron version of the WFAT for the eigenfunctions  $\Psi_A$  and  $\Psi_B$  of the HOMO in a static field. The asymmetries  $a$  were calculated within the WFAT, but calculating the Stark shifts with non-perturbative multi-electron methods (see text for further details).**

	$a'_A$	$a'_B$	$a_A$	$a_B$
CH <sub>3</sub> F	0.75	0.68	0.69	0.58
CH <sub>3</sub> Cl	0.66	0.28	-0.01	-0.45
CH <sub>3</sub> Br	0.23	-0.12	-0.20	-0.46
CH <sub>3</sub> I	-0.29	-0.35	-0.39	-0.43

The asymmetries  $a'$ , calculated within the single-active-electron approximation, predict that  $\text{CH}_3\text{F}$ ,  $\text{CH}_3\text{Cl}$  and  $\text{CH}_3\text{Br}$  all preferentially ionize via the methyl group whereas this preference only reverts for  $\text{CH}_3\text{I}$ . This prediction contrasts with the measured asymmetry  $\alpha$  (Eq. 4) of the  $\text{CH}_3\text{X}^{2+} \rightarrow \text{CH}_3^+ + \text{X}^+$  channel generating low-energy  $\text{CH}_3^+$  fragments. Indeed,  $\text{CH}_3\text{F}$  is the only molecule of this series that preferentially ionizes via the methyl group. In contrast, the asymmetries  $a$  correctly predict the experimentally observed asymmetries for all molecules, i.e. the fact that  $\text{CH}_3\text{Cl}$ ,  $\text{CH}_3\text{Br}$  and  $\text{CH}_3\text{I}$  all preferentially ionize via the halogen atom.

Comparing the modulation amplitude of the emission asymmetry shown in the right panels of Figs. 2a-d for fragment energies below 4 eV one can conclude that the absolute value of the ionization asymmetry of  $\text{CH}_3\text{F}$  is higher compared to the other methyl halides. This aspect is also correctly predicted by the WFAT asymmetries  $a$ . The good agreement between the calculated ionization asymmetry and the emission asymmetry of the  $\text{CH}_3^+$  fragments confirms the assumption that the ionization asymmetry is the decisive quantity defining the asymmetry of the low-energy fragments from the  $\text{CH}_3\text{X}^{2+} \rightarrow \text{CH}_3^+ + \text{X}^+$  Coulomb explosion of the molecules.

As mentioned above, the observed reversals of the emission asymmetry of high-energy  $\text{CH}_3^+$  ions from  $\text{CH}_3\text{Cl}$ ,  $\text{CH}_3\text{Br}$  and  $\text{CH}_3\text{I}$  might be attributed to ionization from lower-lying orbitals. We now investigate this hypothesis by studying the ionization asymmetries of HOMO-1 and HOMO-2. A selection of field-free valence orbitals of the four methyl halides are shown in Fig. 7. The asymmetries  $a$  predict that  $\text{CH}_3\text{F}$  ionizes faster if the electron is removed via the methyl side (i.e. the electric field pointing from  $\text{CH}_3$  to F) where the electron density of the HOMO is maximal (see Fig. 7). In contrast  $\text{CH}_3\text{Cl}$ ,  $\text{CH}_3\text{Br}$  and  $\text{CH}_3\text{I}$  preferentially ionize from the halogen atom, in agreement with the dominant amplitude of the HOMO. Hence, the orbital structure is found to dominate over the Stark effect in the case of HOMO. Considering tunneling ionization from HOMO-1 of the methyl halides (Fig. 7) a smaller ionization asymmetry is expected to be observed due to the symmetric

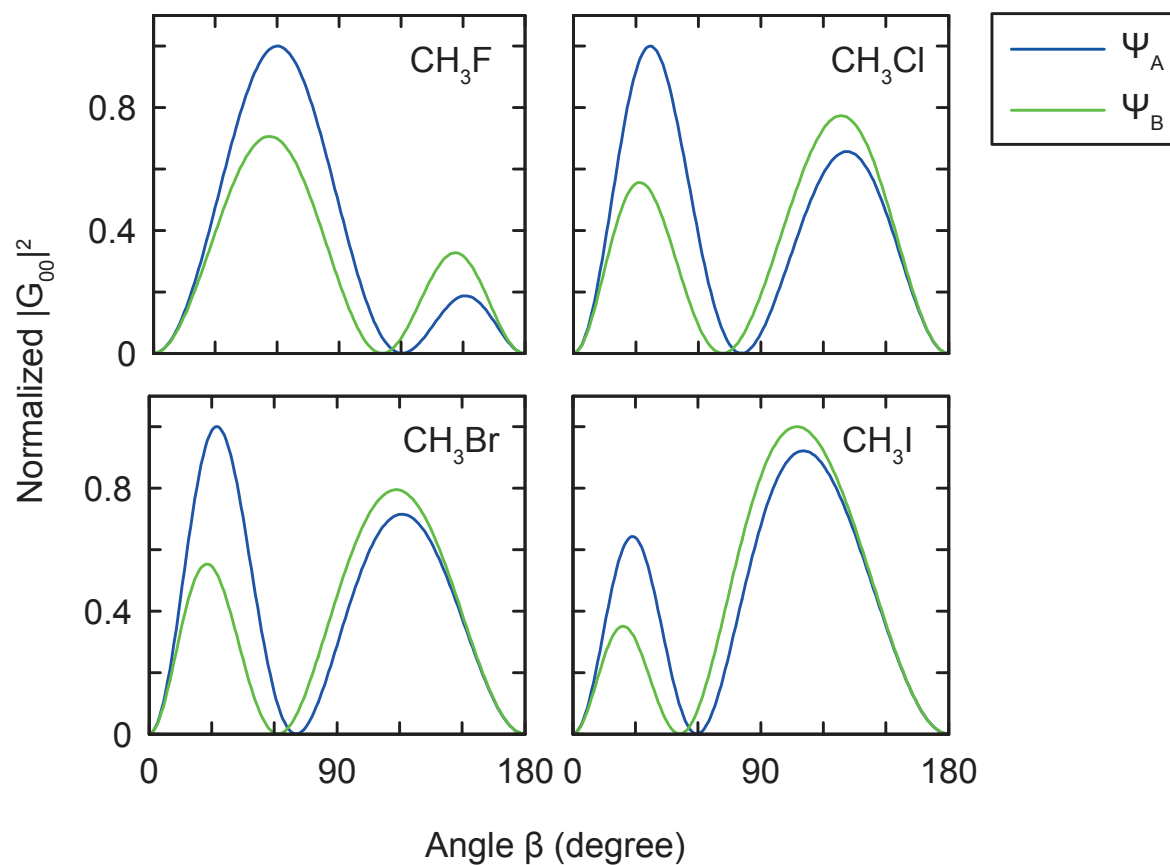


Figure 6: **Calculated ionization rates of the HOMO.** Angle-dependent structure factor  $|G_{00}(\beta, \gamma)|^2$  integrated over  $\gamma$  for the methyl halides.  $|G_{00}(\beta, \gamma)|^2$  was calculated for the two degenerate eigenfunctions  $\Psi_A$  and  $\Psi_B$  individually. For  $\beta = 0^\circ$  the electron is removed from the methyl side.

shape of the orbital. Indeed, the calculated ionization asymmetries  $a$  for HOMO-1 given in Table 5 are smaller compared to those of the HOMO. The calculations predict positive ionization asymmetries  $a$  for HOMO-1 of all 4 molecules. For HOMO-2 positive ionization asymmetries are obtained for both eigenfunctions (see Table 6) except for  $\text{CH}_3\text{Cl}$  for which  $a_B$  is negative but close to zero whereas  $a_A = 0.20$ . Hence, one can conclude that for all methyl halides ionization from HOMO-2 is enhanced if the electron is removed via the methyl end. According to the shape of the field-free HOMO-2 this is again expected because the largest orbital amplitude is at the methyl side.

Our calculations thus predict that the sign of the ionization asymmetry of  $\text{CH}_3\text{F}$  is identical for ionization from the HOMO, HOMO-1 and HOMO-2. This is consistent with the absence of reversals in the emission asymmetry for  $\text{CH}_3^+$  ions from  $\text{CH}_3\text{F}$ . For  $\text{CH}_3\text{Cl}$ ,  $\text{CH}_3\text{Br}$  and  $\text{CH}_3\text{I}$ , where reversals of the emission asymmetry were observed, the sign of the calculated ionization asymmetries obtained for the HOMO are different from the asymmetries obtained for lower lying orbitals. Therefore, it is likely that the changes of the emission asymmetry of the high-energy  $\text{CH}_3^+$  fragments are due to ionization from low-lying orbitals,<sup>49-51</sup> leading to electronically excited states of  $\text{CH}_3\text{X}^{2+}$  and  $\text{CH}_3\text{X}^{3+}$ . In this context, the asymmetry in the  $\text{CH}_3^+$  from  $\text{CH}_3\text{I}$  at 8.3 eV (see Fig. 5) may be assigned to ionization from HOMO and

**Table 5: Similar to Tab. 4 but for HOMO-1.**

	$a'$	$a$
$\text{CH}_3\text{F}$	0.85	0.22
$\text{CH}_3\text{Cl}$	0.55	0.13
$\text{CH}_3\text{Br}$	0.28	0.50
$\text{CH}_3\text{I}$	-0.07	0.05

**Table 6: Similar to Tab. 4 but for HOMO-2.**

	$a'_A$	$a'_B$	$a_A$	$a_B$
$\text{CH}_3\text{F}$	0.75	0.63	0.35	0.12
$\text{CH}_3\text{Cl}$	-0.64	-0.72	0.20	-0.04
$\text{CH}_3\text{Br}$	-0.81	-0.85	0.30	0.06
$\text{CH}_3\text{I}$	-0.91	-0.93	0.49	0.25



HOMO-2, which has a similar but opposite ionization asymmetry as compared to HOMO. HOMO-1, in contrast, has too small an ionization asymmetry to overturn the asymmetry imposed by HOMO. Ionization from HOMO-2 could occur sequentially to ionization from HOMO or through re-collision. An improved theoretical analysis of these results will require the treatment of sequential ionization, electron re-collision and nuclear dynamics.

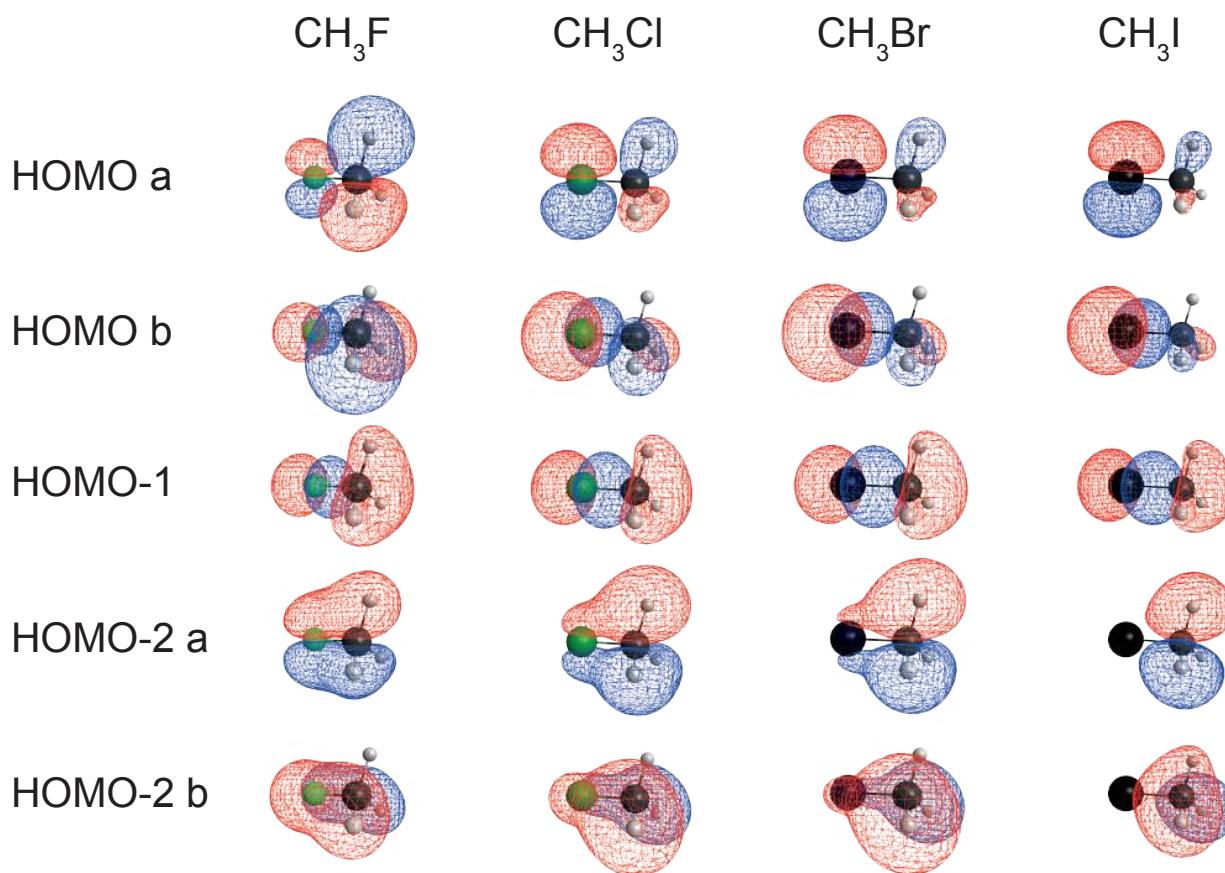


Figure 7: **Isocountour representations of the field-free HOMO, HOMO-1 and HOMO-2 of the methyl halides.** The color indicates the sign of the wave function. The HOMO and HOMO-2 are doubly degenerate and are labeled with a and b, according to Eq. (10). The orbital wave functions were calculated using the quantum chemistry program GAMESS (Version 11; method: restricted HF; basis set: aug-ccpVQZ for  $\text{CH}_3\text{F}$ ,  $\text{CH}_3\text{Cl}$  and  $\text{CH}_3\text{Br}$ ; Def2-QZVP for  $\text{CH}_3\text{I}$ ).

## Conclusion

We have measured the asymmetric emission of charged fragments from methyl halides in intense phase-controlled two-color fields for a range of laser intensities. From the emission asymmetry of the low-energy  $\text{CH}_3^+$  fragments measured at moderate laser intensities we conclude that SFI of  $\text{CH}_3\text{F}$  maximizes when the electric field points from the methyl group to the halogen atom whereas for  $\text{CH}_3\text{Cl}$ ,  $\text{CH}_3\text{Br}$  and  $\text{CH}_3\text{I}$  SFI preferentially proceeds in the opposite direction. We attribute this result to the asymmetric ionization rate of the HOMO of the neutral methyl halide molecules. This conclusion also agrees with the ionization rate predicted by the WFAT, provided that the Stark effect is obtained from non-perturbative multi-electron calculations with applied electric fields. Further we have observed changes of the emission asymmetries of  $\text{CH}_3^+$  fragments from  $\text{CH}_3\text{Cl}$ ,  $\text{CH}_3\text{Br}$  and  $\text{CH}_3\text{I}$  as a function of the kinetic-energy release. We propose that these changes of the asymmetry result from ionization to electronically-excited states of the doubly and triply-charged parent molecules, e.g. by ionization from HOMO and HOMO-2. This assignment is supported by the calculated ionization asymmetries for these orbitals. Further theoretical developments and modelling are required to fully establish this aspect.

## Acknowledgments

S. G. W., A. C. and H. J. W. gratefully acknowledge funding from the Swiss National Science Foundation (200021\_138158), ETH Zürich and an ERC Starting Grant (Project No. 307270-ATTOSCOPE). N. B. R. acknowledges support from a Swiss Government Excellence Scholarship. O. I. T. acknowledges the support from the Ministry of Education and Science of Russia (State Assignment No. 3.679.2014/K). L. B. M. was supported by the ERC-StG (Project No. 277767-TDMET), and the VKR Center of Excellence, QUSCOPE.

## References

- (1) Itatani, J.; Levesque, J.; Zeidler, D.; Niikura, H.; Pépin, H.; Kieffer, J. C.; Corkum, P. B.; Villeneuve, D. M. Tomographic Imaging of Molecular Orbitals. *Nature* **2004**, *432*, 867-871.
- (2) Baker, S.; Robinson, J. S.; Haworth, C. A.; Teng, H.; Smith, R. A.; Chiril, C. C.; Lein, M.; Tisch, J. W. G.; Marangos, J. P. Probing Proton Dynamics in Molecules on an Attosecond Time Scale. *Science* **2006**, *312*, 424-427.
- (3) Haessler, S.; Caillat, J.; Boutu, W.; Giovanetti-Teixeira, C.; Ruchon, T.; Auguste, T.; Diveki, Z.; Breger, P.; Maquet, A.; Carré, B. *et al.* Attosecond Imaging of Molecular Electronic Wavepackets. *Nat. Phys.* **2010**, *6*, 200-206.
- (4) Wörner, H. J.; Bertrand, J. B.; Kartashov, D. V.; Corkum, P. B.; Villeneuve, D. M. Following a Chemical Reaction using High-Harmonic Interferometry. *Nature* **2010**, *466*, 604-607.
- (5) Wörner, H. J.; Bertrand, J. B.; Fabre, B.; Higuette, J.; Ruf, H.; Dubrouil, A.; Patchkovskii, S.; Spanner, M.; Mairesse, Y.; Blanchet, V. *et al.* Conical Intersection Dynamics in NO<sub>2</sub> Probed by Homodyne High-Harmonic Spectroscopy. *Science* **2011**, *334*, 208-212.
- (6) Kraus, P. M.; Baykusheva, D.; Wörner, H. J. Two-Pulse Field-Free Orientation Reveals Anisotropy of Molecular Shape Resonance. *Phys. Rev. Lett.* **2014**, *113*, 023001.
- (7) Okunishi, M.; Morishita, T.; Prümper, G.; Shimada, K.; Lin, C. D.; Watanabe, S.; Ueda, K. Experimental Retrieval of Target Structure Information from Laser-Induced Rescattered Photoelectron Momentum Distributions. *Phys. Rev. Lett.* **2008**, *100*, 143001.
- (8) Ray, D.; Ulrich, B.; Bocharova, I.; Maharjan, C.; Ranitovic, P.; Gramkow, B.; Magrakvelidze, M.; De, S.; Litvinyuk, I. V.; Le, A. T. *et al.* Large-Angle Electron Diffraction

- tion Structure in Laser-Induced Rescattering from Rare Gases. *Phys. Rev. Lett.* **2008**, *100*, 143002.
- (9) Meckel, M.; Comtois, D.; Zeidler, D.; Pavii, D.; Bandulet, H. C.; Pépin, H.; Kieffer, J. C.; Dorner, R.; Villeneuve, D. M.; Corkum, P. B. Laser-Induced Electron Tunneling and Diffraction. *Science* **2008**, *320*, 1478-1482.
- (10) Blaga, C. I.; Xu, J.; DiChiara, A. D.; Sistrunk, E.; Zhang, K.; Agostini, P.; Miller, T. A.; DiMauro, L. F.; Lin, C. D. Imaging Ultrafast Molecular Dynamics with Laser-Induced Electron Diffraction. *Nature* **2012**, *483*, 194-197.
- (11) Bian, X.-B.; Huismans, Y.; Smirnova, O.; Yuan, K.-J.; Vrakking, M. J. J.; Bandrauk, A. D. Subcycle Interference Dynamics of Time-Resolved Photoelectron Holography with Mid-Infrared Laser Pulses. *Phys. Rev. A* **2011**, *84*, 043420.
- (12) Hickstein, D. D.; Ranitovic, P.; Witte, S.; Tong, X.-M.; Huismans, Y.; Arpin, P.; Zhou, X.; Keister, K. E.; Hogle, C. W.; Zhang, B. *et al.* Direct Visualization of Laser-Driven Electron Multiple Scattering and Tunneling Distance in Strong-Field Ionization. *Phys. Rev. Lett.* **2012**, *109*, 073004.
- (13) Meckel, M.; Staudte, A.; Patchkovskii, S.; Villeneuve, D. M.; Corkum, P. B.; Dörner, R.; Spanner, M. Signatures of the Continuum Electron Phase in Molecular Strong-Field Photoelectron Holography. *Nat. Phys.* **2014**, *10*, 594-600.
- (14) Tong, X. M.; Zhao, Z. X.; ; Lin, C. D. Theory of Molecular Tunneling Ionization. *Phys. Rev. A* **2002**, *66*, 033402.
- (15) Muth-Böhm, J.; Becker, A.; Faisal, F. H. M. Suppressed Molecular Ionization for a Class of Diatomics in Intense Femtosecond Laser Fields. *Phys. Rev. Lett.* **2000**, *85*, 2280.

- (16) Computational Chemistry Comparison and Benchmark DataBase - Release 17b, NIST (<http://cccbdb.nist.gov>). Accessed November 2015.
- (17) Tolstikhin, O. I.; Morishita, T.; Madsen, L. B. Theory of Tunneling Ionization of Molecules: Weak-Field Asymptotics Including Dipole Effects. *Phys. Rev. A* **2011**, *84*, 053423.
- (18) Madsen, L. B.; Tolstikhin, O. I.; ; Morishita, T. Application of the Weak-Field Asymptotic Theory to the Analysis of Tunneling Ionization of Linear Molecules. *Phys. Rev. A* **2012**, *85*, 053404.
- (19) Trinh, V. H.; Tolstikhin, O. I.; Madsen, L. B.; ; Morishita, T. First-Order Correction Terms in the Weak-Field Asymptotic Theory of Tunneling Ionization. *Phys. Rev. A* **2013**, *87*, 043426.
- (20) Trinh, V. H.; Pham, V. N. T.; Tolstikhin, O. I.; Morishita, T. Weak-Field Asymptotic Theory of Tunneling Ionization Including the First-Order Correction Terms: Application to Molecules. *Phys. Rev. A* **2015**, *91*, 063410.
- (21) Otobe, T.; Yabana, K.; Iwata, J.-I. First-Principles Calculations for the Tunnel Ionization Rate of Atoms and Molecules. *Phys. Rev. A* **2004**, *69*, 053404.
- (22) Fowe, E. P.; Bandrauk, A. D. Nonperturbative Time-Dependent Density-Functional Theory of Ionization and Harmonic Generation in OCS and CS<sub>2</sub> Molecules with Ultra-short Intense Laser Pulses: Intensity and Orientational Effects. *Phys. Rev. A* **2011**, *84*, 035402.
- (23) Zhang, B.; Yuan, J.; Zhao, Z. Dynamic Core Polarization in Strong-Field Ionization of CO Molecules. *Phys. Rev. Lett.* **2013**, *111*, 163001.
- (24) Petretti, S.; Vanne, Y. V.; Saenz, A.; Castro, A.; Decleva, P. Alignment-Dependent

- Ionization of N<sub>2</sub>, O<sub>2</sub>, and CO<sub>2</sub> in Intense Laser Fields. *Phys. Rev. Lett.* **2010**, *104*, 223001.
- (25) Majety, V. P.; Zielinski, A.; Scrinzi, A. Photoionization of Few Electron Systems: A Hybrid Coupled Channels Approach. *New J. Phys.* **2015**, *17*, 063002.
- (26) Holmegaard, L.; Hansen, J. L.; Kahlj, L.; Kragh, S. L.; Stapelfeldt, H.; Filsinger, F.; Küpper, J.; Meijer, G.; Dimitrovski, D.; Abu-samha, M. *et al.* Photoelectron Angular Distributions from Strong-Field Ionization of Oriented Molecules. *Nat. Phys.* **2010**, *6*, 428-432.
- (27) Dimitrovski, D.; Martiny, C. P. J.; Madsen, L. B. Strong-Field Ionization of Polar Molecules: Stark-Shift-Corrected Strong-Field Approximation. *Phys. Rev. A* **2010**, *82*, 053404.
- (28) Dimitrovski, D.; Abu-samha, M.; Madsen, L. B.; Filsinger, F.; Meijer, G.; Küpper, J.; Holmegaard, L.; Kahlj, L.; Nielsen, J. H.; Stapelfeldt, H. Ionization of Oriented Carbonyl Sulfide Molecules by Intense Circularly Polarized Laser Pulses. *Phys. Rev. A* **2011**, *83*, 023405.
- (29) Hansen, J. L.; Holmegaard, L.; Nielsen, J. H.; Stapelfeldt, H.; Dimitrovski, D.; Madsen, L. B. Orientation-Dependent Ionization Yields from Strong-Field Ionization of Fixed-in-Space Linear and Asymmetric Top Molecules. *J. Phys. B: At., Mol. Opt. Phys.* **2012**, *45*, 015101.
- (30) Kraus, P. M.; Rupenyan, A.; Wörner, H. J. High-Harmonic Spectroscopy of Oriented OCS Molecules: Emission of Even and Odd Harmonics. *Phys. Rev. Lett.* **2012**, *109*, 233903.
- (31) Ohmura, H.; Saito, N.; ; Morishita, T. Molecular Tunneling Ionization of the Carbonyl Sulfide Molecule by Double-Frequency Phase-Controlled Laser Fields. *Phys. Rev. A* **2014**, *89*, 013405.

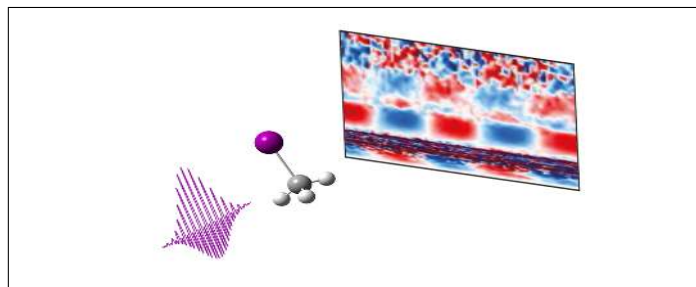
- (32) Madsen, L. B.; Jensen, F.; Tolstikhin, O. I.; ; Morishita, T. Structure Factors for Tunneling Ionization Rates of Molecules. *Phys. Rev. A* **2013**, *87*, 013406.
- (33) Ohmura, H.; Ito, F.; Tachiya, M. Phase-Sensitive Molecular Ionization Induced by a Phase-Controlled Two-Color Laser Field in Methyl Halides. *Phys. Rev. A* **2006**, *74*, 043410.
- (34) Thompson, M. R.; Thomas, M. K.; Taday, P. F.; Posthumus, J. H.; Langley, A. J.; Frasinski, L. J.; Codling, K. One and Two-Color studies of the Dissociative Ionization and Coulomb Explosion of H<sub>2</sub> with Intense Ti:Sapphire Laser Pulses. *J. Phys. B: At. Mol. Opt. Phys.* **1997**, *30*, 5755.
- (35) Ray, D.; He, F.; De, S.; Cao, W.; Mashiko, H.; Ranitovic, P.; Singh, K. P.; Znakovskaya, I.; Thumm, U.; Paulus, G. G. *et al.* Ion-Energy Dependence of Asymmetric Dissociation of D<sub>2</sub> by a Two-Color Laser Field. *Phys. Rev. Lett.* **2009**, *103*, 223201.
- (36) Sheehy, B.; Walker, B.; DiMauro, L. F. Phase Control in the Two-Color Photodissociation of HD<sup>+</sup>. *Phys. Rev. Lett.* **1995**, *74*, 4799.
- (37) Li, H.; Ray, D.; De, S.; Znakovskaya, I.; Cao, W.; Laurent, G.; Wang, Z.; Kling, M. F.; Le, A. T.; Cocke, C. L. Orientation Dependence of the Ionization of CO and NO in an Intense Femtosecond Two-Color Laser Field. *Phys. Rev. A* **2011**, *84*, 043429.
- (38) Ohmura, H.; Saito, N.; Tachiya, M. Selective Ionization of Oriented Nonpolar Molecules with Asymmetric Structure by Phase-Controlled Two-Color Laser Fields. *Phys. Rev. Lett.* **2006**, *96*, 173001.
- (39) Ohmura, H.; Saito, N.; Nonaka, H.; Ichimura, S. Dissociative Ionization of a Large Molecule Studied by Intense Phase-Controlled Laser Fields. *Phys. Rev. A* **2008**, *77*, 053405.

- (40) Walt, S. G. Imaging Electronic Structure and Dynamics of Molecules through Strong-Field Ionization, Rescattering and Holography. Ph.D. Thesis, ETH Zurich, **2015**.
- (41) Vrakking, M. J. J. An Iterative Procedure for the Inversion of Two-Dimensional Ion/Photoelectron Imaging Experiments. *Rev. Sci. Instrum.* **2001**, *72*, 4084-4089.
- (42) Corrales, M. E.; Gitzinger, G.; González-Vázquez, J.; Loriot, V.; de Nalda, R.; Banares, L. Velocity Map Imaging and Theoretical Study of the Coulomb Explosion of CH<sub>3</sub>I under Intense Femtosecond IR Pulses. *J. Phys. Chem. A* **2011**, *116*, 2669-2677.
- (43) Liu, H.; Yang, Z.; Gao, Z.; Tang, Z. Ionization and Dissociation of CH<sub>3</sub>I in Intense Laser Field. *J. Chem. Phys.* **2007**, *126*, 044316.
- (44) Sun, S.; Yang, Y.; Zhang, J.; Wu, H.; Chen, Y.; Zhang, S.; Jia, T.; Wang, Z.; Sun, Z. Ejection of Triatomic Molecular Ion H<sub>3</sub><sup>+</sup> Image from Methyl Chloride in an Intense Femtosecond Laser Field. *Chem. Phys. Lett.* **2013**, *581*, 16-20.
- (45) Kotsina, N.; Kaziannis, S.; Kosmidis, C. Hydrogen Migration in Methanol Studied under Asymmetric fs Laser Irradiation. *Chem. Phys. Lett.* **2014**, *604*, 27-32.
- (46) Tanaka, M.; Murakami, M.; Yatsunami, T.; Nakashima, N. Atomic-like Ionization and Fragmentation of a Series of CH<sub>3</sub>X (X: H, F, Cl, Br, I, and CN) by an Intense Femtosecond Laser. *J. Chem. Phys.* **2007**, *127*, 104314.
- (47) Kraus, P. M.; Tolstikhin, O. I.; Baykusheva, D.; Rupenyan, A.; Schneider, J.; Bisgaard, C. Z.; Morishita, T.; Jensen, F.; Madsen, L. B.; Wörner, H. J. Observation of Laser-Induced Electronic Structure in Oriented Polyatomic Molecules. *Nat. Commun.* **2015**, *6*, 7039.
- (48) Tolstikhin, O. I.; Madsen, L. B.; Morishita, T. Weak-Field Asymptotic Theory of Tunneling Ionization in Many-Electron Atomic and Molecular Systems. *Phys. Rev. A* **2014**, *89*, 013421.



- (49) Akagi, H.; Otobe, T.; Staudte, A.; Shiner, A.; Turner, F.; Dörner, R.; Villeneuve, D. M.; Corkum, P. B. Laser Tunnel Ionization from Multiple Orbitals in HCl. *Science* **2009**, *325*, 1364-1367.
- (50) Wu, J.; Schmidt, L. P. H.; Kunitski, M.; Meckel, M.; Voss, S.; Sann, H.; Kim, H.; Jahnke, T.; Czasch, A.; Dörner, R. Multiorbital Tunneling Ionization of the CO Molecule. *Phys. Rev. Lett.* **2012**, *108*, 183001.
- (51) Liu, H.; Zhao, S.-F.; Li, M.; Deng, Y.; Wu, C.; Zhou, X.-X.; Gong, Q.; ; Liu, Y. Molecular-Frame Photoelectron Angular Distributions of Strong-Field Tunneling from Inner Orbitals. *Phys. Rev. A* **2013**, *88*, 061401.

## Graphical TOC Entry



Asymmetries of dissociative ionization and Coulomb explosion of the methyl halides in two-color laser fields.